

Observing the Accretion Stream in Polars

Jens Kube, Boris T. Gänsicke, Klaus Beuermann

Universitäts-Sternwarte, Geismarlandstr. 11, D-37083 Göttingen, Germany

Abstract.

We have developed a 3D computer model of polars which includes the accretion stream, the accretion column, the secondary star, and the white dwarf. Each component is represented by a fine grid of surface elements. With brightness values attributed to each surface element, this model generates synthetic light curves of the various components. As a first application, we present our simulated light curves of the accretion stream, fitted to high-speed HST spectroscopy of the eclipsing polar UZ Fornacis by the means of an evolution strategy.

1. Introduction

Orbital phase-resolved spectroscopy of the bright emission lines in polars provides a unique possibility to derive information on the intensity and velocity distribution along the accretion stream. In eclipsing polars, the geometric constraints allow a direct transformation of an emission line light curve into a brightness map of the accretion stream. We have developed a computer model of polars which includes 3D grid models of the secondary star, the white dwarf, the accretion stream, and the column. Each component is represented by a large number of surface elements, to which brightness values are attributed. We calculate the projected surface area of each element for the desired phase interval and sum up the flux contributions of all surface elements to obtain the total flux emitted in the direction of the observer. This light curve can then be fitted to observations in order to derive intensity maps of the components of the polar. Our present work focuses on the accretion stream, which is the source of the broad emission lines.

2. Synthetic light curves

In Fig. 1 (left) we show a synthetic light curve for the accretion stream in a polar at high inclination, $i = 88^\circ$. The intensity of the white dwarf and the secondary star are set to zero; for simplicity, the accretion stream is assumed to have a uniform surface brightness. Our light curve shows various features, present also in observed systems (e.g. Schwöpe et al., 1997). We follow the features around the orbit (Fig. 1, right): (1) The dipole part of the accretion stream has completely reappeared after the eclipse. (2) The projected area of the accretion stream is maximal. (3) The white dwarf causes a partial eclipse

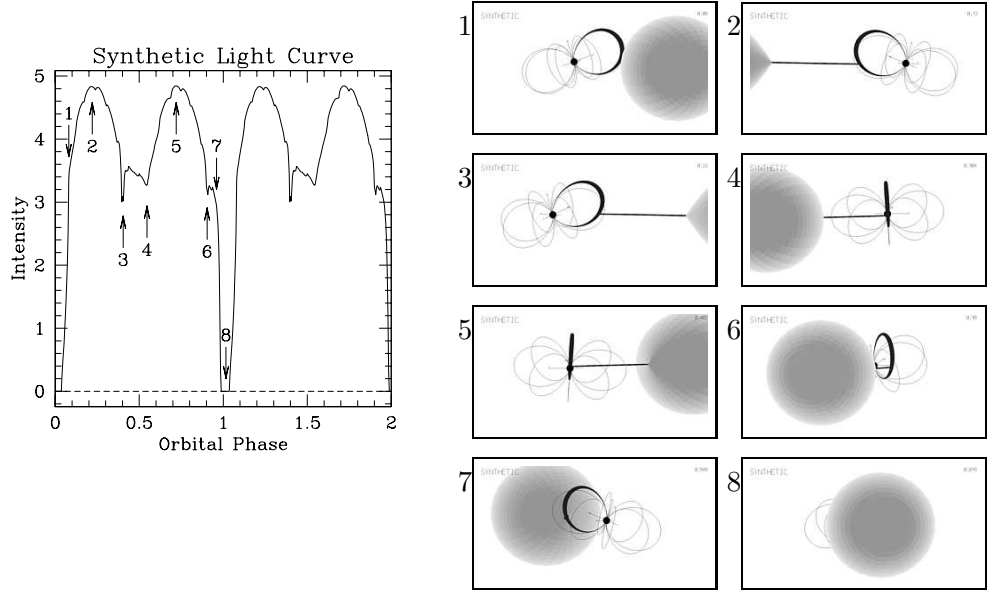


Figure 1. Synthetic light curve of the accretion stream only (left) with various numbered features and corresponding views of the polar (right)

of the accretion stream. (4) A secondary minimum occurs, when the projected area of the ballistic part of the accretion stream is minimal. (5) As in (2), the projected area of the accretion stream is maximal. (6) A dip comes from the self-eclipse of the dipole part of the stream. (7) The main eclipse begins. At first, the stream sections near the L_1 -point disappear, followed by the white dwarf and the dipole stream; at last, the stream sections near the stagnation region are eclipsed. (8) The stream is eclipsed completely. Note that the center of the eclipse of the stream is offset from the center of the eclipse of the white dwarf.

Schwope et al. (1997) presented an observed light curve of the broad-line emission in HU Aqr which represents the emission of the accretion stream and shows the same double-hump shape as our calculated light curve in Fig. 1.

3. Geometry

The accretion stream geometry depends strongly on the tilt and azimuth of the dipole axis, characterized by the angles β and Ψ in Fig. 2. A third characteristic angle is the azimuth of the stagnation region, Ψ_S . These three parameters describe the geometry of the accretion stream under the following assumptions: (1) The width of the stagnation region is given by the dispersion of the free-fall trajectories emerging with a thermal distribution from the L_1 -point (Flannery, 1975). (2) Magnetically funneled accretion occurs along the same field line for the stream above and below the orbital plane. (3) The center of the dipole lies in the center of the white dwarf, i.e. there is no dipole offset.

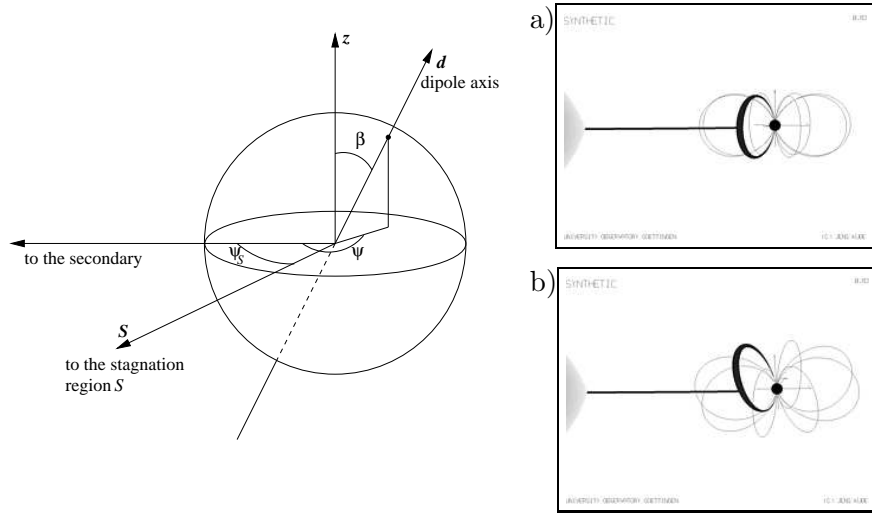


Figure 2. Geometry of the magnetic dipole: definition (left) and examples (right) (a)+(b) $\Psi_S = 35^\circ$, (a) tilt $\beta = 20^\circ$, azimuth $\Psi = 75^\circ$, (b) $\beta = 0^\circ$, $\Psi = 45^\circ$

4. Application: UZ Fornacis

UZ For was observed with HST in June 1992; a detailed description of the data is given by Stockman & Schmidt (1996). We summarize here only the relevant points. Fast FOS/G160L spectroscopy with a time resolution of 1.6914 s was obtained, covering two entire eclipses in the phase interval $\phi = 0.87 \dots 1.07$. The spectra cover the range 1180–2500 Å with a FWHM resolution of ≈ 7 Å. We have retrieved these data from the HST archive at STScI, calibrated with the standard reduction pipeline. The mid-exposure times of the individual spectra were converted into binary orbital phases using the ephemeris of Warren et al. (1995). The two individual observations were then co-added (Fig. 3, left). From this trailed spectrum, we extracted the light curve of C IV $\lambda 1550$ (Fig. 3, right).

We use the system parameters from Bailey & Cropper (1991): $q = M_1/M_2 = 5$, $M = M_1 + M_2 = 0.85 M_\odot$, $i = 81^\circ$, $P = 126.5$ min. The optical light curve in Bailey (1995) shows two eclipse steps which can be explained by two hot spots on the white dwarf which subsequently disappear behind the limb of the secondary star. From that light curve we can measure the timing of the eclipse events with an accuracy of $\Delta\phi = 5 \cdot 10^{-4}$. The ingress of the spot on the lower hemisphere occurs at $\phi = 0.9685$, its egress at $\phi = 1.0310$; for the spot on the upper hemisphere, ingress is at $\phi = 0.9725$ and egress at $\phi = 1.0260$.

In addition to the “basic parameters” mentioned above we derive the following *preliminary* dipole configuration from the hot spot eclipse timings: $\beta = 15^\circ$, $\Psi = -25^\circ$, $\Psi_S = 33^\circ$

Using these parameters, we fit the C IV light curve. Fit parameters are the ≈ 200 brightness values along the stream. The brightness distribution is optimized by an evolution strategy, which is the favourable choice for large numbers of fit parameters. The fit converges after approximately 300 iterations

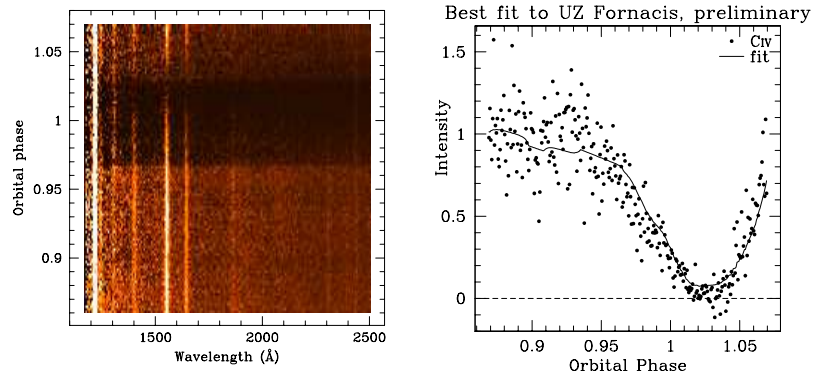


Figure 3. Raw data (left) and extracted light curve with fit (right)

having calculated roughly 30 000 light curves in total. In order to reduce the number of degrees of freedom, we have implemented a smoothing algorithm based on maximum entropy.

Our best fit is shown in Fig. 3 (right). This preliminary fit assumes that accretion to both poles occurs along the same field line. This assumption turns out to be consistent with the position of the lower main accretion spot, but not simultaneously with that of the upper secondary spot. Dropping the assumption of accretion onto both poles on the same field line introduces an additional degree of freedom. The detailed 3D brightness distribution will necessarily change with any additional assumption made and is not shown here. Independent of the remaining uncertainties, however, our fit implies that the accretion stream is brightest near the stagnation region where it couples onto the magnetic field.

5. Summary

Our new model allows light curve synthesis of CVs and tomographical reconstruction of brightness maps by the means of evolution fit strategies. As a first result, we have found that the stagnation region in the magnetosphere of the polar UZ For is a prominent source of emission lines.

References

- Bailey, J. 1995, in *Cape Workshop on Magnetic Cataclysmic Variables*, ASP Conf. Ser. 85, 10
- Bailey, J., Cropper, M. 1991, MNRAS 253, 27
- Flannery, B. P. 1975, MNRAS 170, 325
- Schwope, A., Mantel, K.-H. & Horne, K. 1997, A&A 319, 894
- Stockman, H., Schmidt, G. 1996, ApJ 468, 883
- Warren, J.K., Vallerga, J.V. & Sirk, M.M. 1995 ApJ 445, 909